AGU PUBLICATIONS

JGR

Journal of Geophysical Research: Atmospheres

RESEARCH ARTICLE
10.1002/2017JD026599

Key Points:
- Black carbon in a western Antarctic ice core increased during the mid-Holocene
- Mid-Holocene model simulations show increased fire-driven carbon loss and annual fire season length for three regions in South America
- Black carbon flux to Antarctica parallels low-latitude hydroclimate

Supporting Information:
- Supporting Information S1

Correspondence to:
M. M. Arienzo,
monica.arienzo@dri.edu

Citation:
Arienzo, M. M., J. R. McConnell, L. N. Murphy, N. Chellman, S. Das, S. Kipfstuhl, and R. Mulvaney (2017), Holocene black carbon in Antarctica paralleled Southern Hemisphere climate, *J. Geophys. Res. Atmos.*, *122*, doi:10.1002/2017JD026599.

Received 9 FEB 2017
Accepted 9 JUN 2017
Accepted article online 11 JUN 2017

Holocene black carbon in Antarctica paralleled Southern Hemisphere climate

M. M. Arienzo[1], J. R. McConnell[1], L. N. Murphy[2], N. Chellman[1], S. Das[3], S. Kipfstuhl[4], and R. Mulvaney[5]

[1]Division of Hydrologic Sciences, Desert Research Institute, Reno, Nevada, USA, [2]Department of Atmospheric Sciences, Rosenstiel School of Marine and Atmospheric Science, University of Miami, Miami, Florida, USA, [3]Woods Hole Oceanographic Institution, Woods Hole, Massachusetts, USA, [4]Alfred-Wegener-Institut, Helmholtz-Zentrum für Polar- und Meeresforschung, Bremerhaven, Germany, [5]British Antarctic Survey, Cambridge, UK

Abstract Black carbon (BC) and other biomass-burning (BB) aerosols are critical components of climate forcing, but quantification, predictive climate modeling, and policy decisions have been hampered by limited understanding of the climate drivers of BB and by the lack of long-term records. Prior modeling studies suggested that increased Northern Hemisphere anthropogenic BC emissions increased recent temperatures and regional precipitation, including a northward shift in the Intertropical Convergence Zone (ITCZ). Two Antarctic ice cores were analyzed for BC, and the longest record shows that the highest BC deposition during the Holocene occurred ~8–6 k years before present in a period of relatively high austral burning season and low growing season insolation. Atmospheric transport modeling suggests South America (SA) as the dominant source of modern Antarctic BC and, consistent with the ice core record, climate model experiments using mid-Holocene and preindustrial insolation simulate comparable increases in carbon loss due to fires in SA during the mid-Holocene. SA climate proxies document a northward shifted ITCZ and weakened SA Summer Monsoon (SASM) during this period, with associated impacts on hydroclimate and burning. A second Antarctic ice core spanning the last 2.5 k years documents similar linkages between hydroclimate and BC, with the lowest deposition during the Little Ice Age characterized by a southerly shifted ITCZ and strengthened SASM. These new results indicate that insolation-driven changes in SA hydroclimate and BB, likely linked to the position of the ITCZ, modulated Antarctic BC deposition during most of the Holocene and suggests connections and feedbacks between future BC emissions and hydroclimate.

Plain Language Summary Future anthropogenic-driven climate change may impact wildfires, yet predictions are hampered by few long-term records of natural wildfires, particularly for the Southern Hemisphere. We document large variations in black carbon deposition during the past 14,000 years from an Antarctic ice core. Black carbon is a tracer for wildfires and is a significant climate forcing agent. We show that black carbon in Antarctica closely followed Southern Hemisphere hydroclimate and strength of the South American Summer Monsoon. With future predictions showing significant low-latitude changes in precipitation under increased emissions, the climate-fire linkages presented here suggest future changes to South American biomass burning.

1. Introduction

Black carbon (BC) aerosols emitted from combustion play a critical role in climate forcing. BC forces climate directly by changing Earth's radiation budget [*Bond et al.*, 2013] and indirectly by changing cloud formation and reducing albedo [*Bisiaux et al.*, 2012b; *McConnell et al.*, 2007; *Painter et al.*, 2013]. Studies show that BC is the second most important anthropogenic radiative-forcing agent today, after carbon dioxide [*Bond et al.*, 2013]. Climate model simulations suggest related changes in recent large-scale atmospheric circulation and hydroclimate in response to BC-driven Northern Hemisphere warming, particularly in the Arctic [*Bond et al.*, 2013; *Jones et al.*, 2007; *Shindell and Faluvegi*, 2009].

Biomass burning (BB) is modulated by climatic variations—such as precipitation and temperature [*Westerling et al.*, 2006]—that alter fuel load, flammability, and fuel type [*Marlon et al.*, 2013]. With increased precipitation, burning in wetter regions is thought to decrease while in semiarid regions burning likely increases due to increased fuel loads [*Daniau et al.*, 2013; *Marlon et al.*, 2013; *van der Werf et al.*, 2008]. Since the Last Glacial

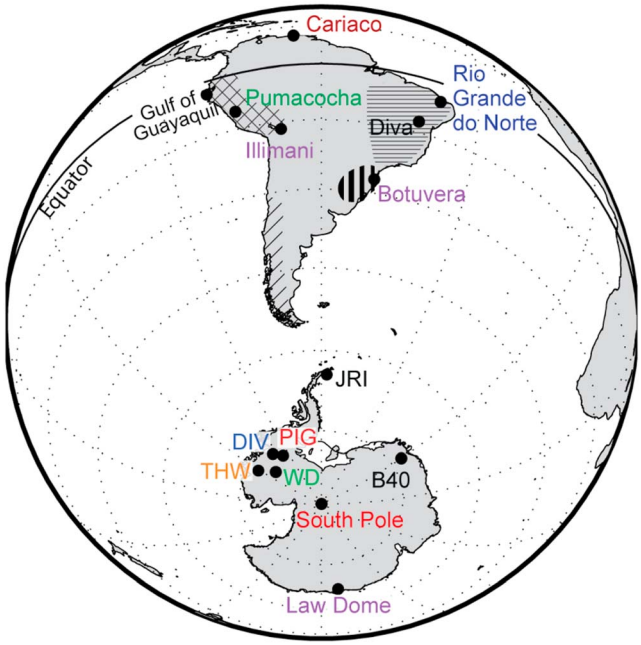

Figure 1. Site map showing locations of the ice cores and the relationships to referenced paleorecords. Shaded areas indicate regions of charcoal record compilations, crosshatches for western Amazonia, diagonal lines for Patagonia, horizontal stripes for eastern Amazonia, and vertical lines for the Pampas region.

Maximum (LGM), temperature is the major driver of changes in BB [*Daniau et al.*, 2012]. Climate-fire linkages are complicated further by humans through direct ignition of fires, and changes in vegetation type and amount [*Daniau et al.*, 2012; *Marlon et al.*, 2008]. BB reconstructions typically made through regional aggregation of lake-sediment charcoal records—each reflecting local burning on the scale of a few kilometers—suggested a potential link between large-scale climate and BB [*Marlon et al.*, 2013]. While studies have demonstrated a connection between anthropogenic-driven changes in BB, BC emission, precipitation, and temperature [*Bond et al.*, 2013; *Westerling et al.*, 2006], understanding of the natural variations and climate drivers of regional-scale BB, BC emissions, and potential climate feedbacks remains limited [*Marlon et al.*, 2013]. Such a link between climate and BB remains tentative because of uncertainties inherent in charcoal-based burning reconstructions arising from local influences, nonuniform spatial and temporal coverage in the underlying charcoal records, and low temporal resolution [*Calder et al.*, 2015].

Far smaller than charcoal fragments, BC aerosols during the preindustrial are primarily sourced from BB and directly impact climate forcing [*Bond et al.*, 2013]. Long-term ice core BC records have provided insights into natural climate-fire relationships [*McConnell et al.*, 2007; *Zennaro et al.*, 2014; *Keegan et al.,* 2014]. In contrast to lake-sediment charcoal records, polar ice core records have subannual to annual resolution, are precisely dated [*Buizert et al.*, 2015; *Sigl et al.*, 2015], do not exhibit postdepositional mixing or alteration of BC, and are located far from BB sources—therefore reflecting regional rather than local burning emissions and large-scale atmospheric BB aerosol concentrations [*Bisiaux et al.*, 2012b; *McConnell et al.*, 2007].

In this study we use BC measurements in two Antarctic ice cores to reconstruct preanthropogenic changes in BC and BB emissions for the Southern Hemisphere. Given the uncertainties for future Southern Hemisphere low-latitude precipitation [*Chadwick et al.*, 2015] and BB [*Moritz et al.*, 2012], BC records and climate simulations across longer timescales are needed. Earth system model simulations indicate that the largest contributor of BC in the modern Southern Hemisphere atmosphere is BB in South America (SA) [*Koch et al.*, 2007], and future predictions suggest that BC emissions will increase from African residential, South American BB, and developing world transportation sources [*Bond et al.*, 2013]. With the importance of BC to climate forcing and to ice sheet albedo [*Bond et al.*, 2013], understanding of past natural linkages between climate, BB, and BC emissions in the Southern Hemisphere is critical for climate model simulations and future predictions.

Here we use continuous, high-resolution measurements of BC in two Antarctic ice cores, West Antarctic Ice Sheet Divide (WD), and B40 to develop Holocene records of Southern Hemisphere BB emissions. These two ice cores document significant changes in BC deposition during the mid-Holocene and Little Ice Age (LIA) potentially related to changes in BB emissions and/or transport from the source. We interpret the distal ice core BC records from WD and B40 using comparisons to climate model simulations and to more proximal stalagmites [*Cruz et al.*, 2009; *Wang et al.*, 2007; *Novello et al.*, 2012] from eastern South America, lake and marine sediments cores [*Bird et al.,* 2011; *Mollier-Vogel et al.,* 2013; *Haug et al.,* 2001] from western South America, and the Illimani ice core record [*Kellerhals et al.*, 2010] from Peru (Figure 1). Long-range transport and atmospheric mixing are implicit in Antarctic records where BC must be transported from middle to low-latitude BB

Table 1. Site Locations for the Seven Ice Cores Presented in This Study and Recent Accumulation

Site	Latitude (deg min s)	Longitude (deg min s)	Recent Accumulation (kg m^{-2} yr^{-1})
B40	70°0′S	0°3′36″E	68
DIV	76°46′13″ S	101°44′15″W	372
JRI	64°12′S	57°42′W	530
Law Dome	66°44′S	112°50′E	150
PIG	77°57′25″S	95°57′42″W	403
THW	76°57′9″S	121°13′13″W	274
WD	79°28′S	112°4′W	200

sources across the Southern Ocean, so comparisons to more proximal records are important for distinguishing between source-emission changes and atmospheric-transport processes.

2. Methods

2.1. Ice Core Collection

We measured BC and ammonium (NH_4^+) in the ice cores using the well-established Desert Research Institute's (DRI's) continuous ice core melter system [*Bisiaux et al.*, 2012b; *McConnell et al.*, 2002, 2007; *Pasteris et al.*, 2014a, 2014b; *Zennaro et al.*, 2014]. We report the Holocene record of BC (14 k to 2.475 k years before 1950 [yr B.P.]) measured in the 3404 m WD ice core (79°28′S, 112°4′W, 1,766 m elevation) [*Buizert et al.*, 2015; *Sigl et al.*, 2015] (Figure 1 and Table 1), and BC and NH_4^+ for the more recent past (2.485 k yr B.P. to present) measured in the 200 m East Antarctic B40 ice core (70°0′S, 0°3′36″E) drilled in 2013 Common Era (C.E.) [*McConnell et al.*, 2014] (Figure 1). Contiguous, continuous measurements of the entire 200 m B40 core and from 2190 to 1302 m in the WD core were conducted. Additionally, continuous measurements were made on ~20 m contiguous sections taken every ~220 m from 1282 to 576 m in the brittle ice zone at WD (Figures 2 and 3).

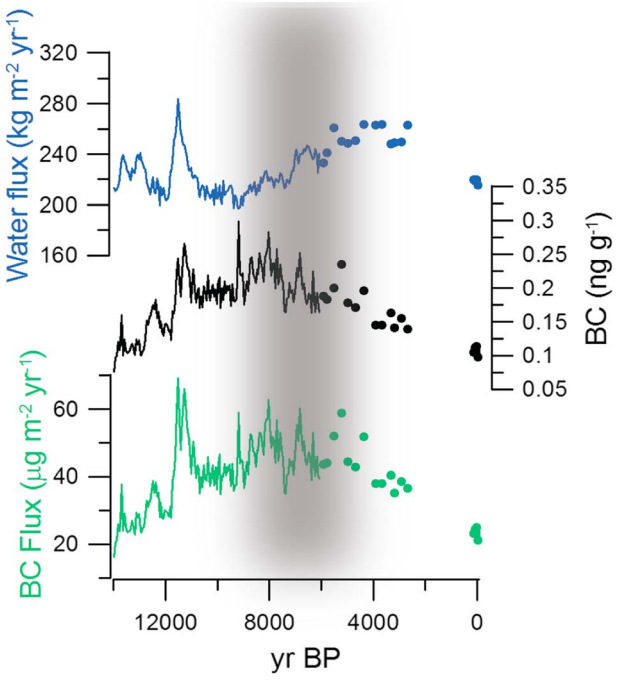

Figure 2. The 50 year averaged water flux (blue), BC concentration (black), and BC flux (green) for WD ice core. The measurements demonstrate that most of the Holocene BC flux variability results from changes in concentration, not water (snow) accumulation. Measurements in the brittle ice zone are shown as circles. Measurements over the past 150 years are from *Bisiaux et al.* [2012b]. Gray bar represents the period of increased BC deposition during the mid-Holocene. Increased BC flux at ~11 k yr B.P. is thought to be due to increased water accumulation.

Both cores were collected at cold, dry-snow sites with little or no surface melting. Recent accumulation rates were 68 kg m^{-2} yr^{-1} and 200 kg m^{-2} yr^{-1} for B40 [*McConnell et al.*, 2014] and WD [*Banta et al.*, 2008], respectively (Table 1). The strong seasonality in many parameters allowed for annual-layer counting with minimal uncertainty in the high snow accumulation WD record, and the WD2014 timescale was used [*Buizert et al.*, 2015; *Sigl et al.*, 2015, 2016]. Annual-layer counting for the top 30,000 years is described in *Sigl et al.* [2016]. Age accuracy estimates for the WD2014 timescale as reported by *Sigl et al.* [2016] are better than 0.5% of the age from 11 k yr B.P. and younger and increases to 1% of the age beyond 14.5 k yr B.P. Annual-layer counting also was conducted on the B40 record and was constrained by synchronization to the WD record using distinct volcanic markers [*Sigl et al.*, 2014]. For ice cores, annual-layer identification is best

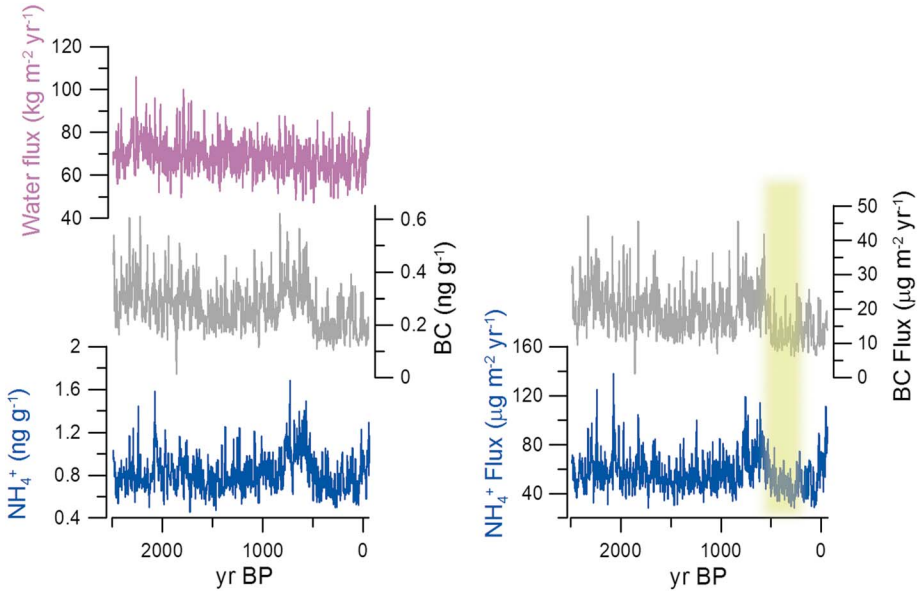

Figure 3. BB tracers from the B40 ice core. (left) Water flux in purple, BC concentration in gray, and ammonium (NH_4^+) concentration in blue. (right) BC flux in gray and NH_4^+ flux in blue. Shown are 7 year medians. Measurements show that most of the variability during the past 2500 years results from changes in concentration, not water (snow) accumulation. Yellow bar represents the period of decreased BC flux in B40.

conducted by a robust seasonal indicator, for example, the maxima in the non-sea-salt sulfur to sodium (nssS/Na) ratio which occurs in the midsummer as a result of high summer marine biogenic sulfur aerosol emissions [*Sigl et al.*, 2016]. From these annual picks, seasonality in both WD and B40 was determined assuming a constant rate of snow accumulation between annual markers [*Sigl et al.*, 2016]. While there may be year-to-year variations in snow accumulation seasonality [*Rhodes et al.*, 2017], we have averaged 1000 years of seasonally resolved measurements for both the WD and B40 ice cores for nssS/Na, BC, and NH_4^+ (Figure 4) to reduce intra-annual variability in snow accumulation. Depositional fluxes were calculated from BC (Figures 2 and 3) and NH_4^+ concentrations (Figure 3) using each year's water-equivalent accumulation derived from annual-layer counting [*Sigl et al.*, 2015, 2016] and measured density profiles, with flow thinning corrections based on ice sheet modeling [*Buizert et al.*, 2015].

2.2. Black Carbon and Ammonium

The DRI method for continuous BC and NH_4^+ determinations in ice cores has been described previously [*Bisiaux et al.*, 2012a; *Pasteris et al.*, 2014a, 2014b]. Prior to analysis, longitudinal samples with a cross section of ~0.032 by ~0.032 m from the two ice cores were cut and the ends decontaminated by scraping with a precleaned ceramic knife. The DRI BC method used in the analysis of B40 and WD coupled a Cetac U5000AT Ultrasonic Nebulizer (USN) to a Single Particle Soot Photometer (SP2; Droplet Measurement Technologies, Boulder, CO, USA) for high-time-resolution, continuous determinations of BC concentration in real time since measurements were made approximately 3 min after the ice core was melted. Implicit in the original DRI method were mass-dependent nebulization efficiencies associated with the Cetac USN that may result in a slight bias toward smaller particles [*Lim et al.*, 2014]. The impact on concentration measurements depends on the relative distributions in standards and samples for particle-mass-equivalent diameters of $>$350 nm [*Wendl et al.*, 2014]. The impact of nebulization efficiency was small in Antarctica where long-range transport from middle and low-latitude source regions across the Southern Ocean favors smaller particles, leading to ~20% smaller BC particle-mass distributions and ~90% lower concentrations than those typically found in Greenland ice [*McConnell et al.*, 2007]. This resulted in similar BC particle sizes in Antarctic ice cores and the Cabojet 200 black carbon standard (Cabot Corporation, Boston, MA, USA). Comparisons between measurements of 6 m of parallel B40 ice core samples using the Cetac USN and the Apex Q jet-type nebulizer (Elemental Scientific, Omaha, Nebraska, USA) showed that concentrations differed by $<$5% (Figure S1 in the supporting information).

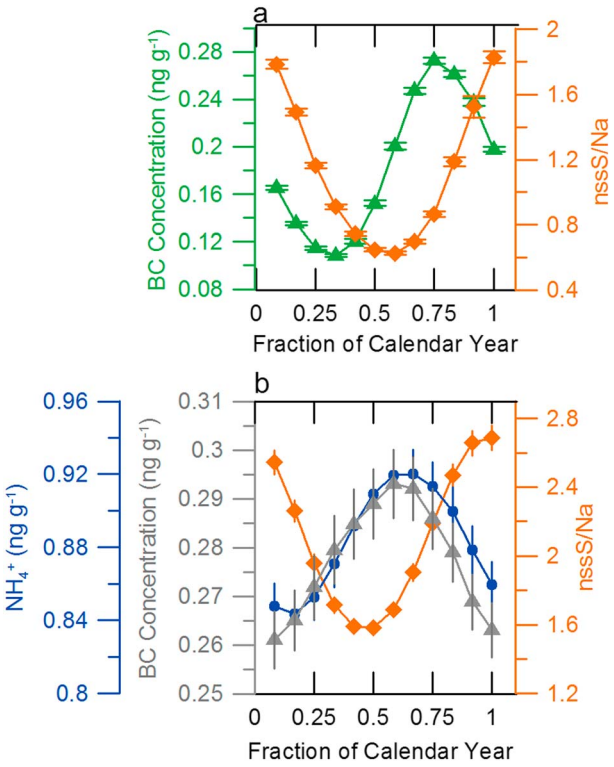

Figure 4. Approximate seasonality of BC and other aerosol concentrations in Antarctic ice cores. (a) Average cycles for BC (green) and nssS/Na ratio (orange) for the millennium between 8.0 k and 7.0 k yr B.P. in the WD record. (b) Average cycles for BC (gray triangles), nssS/Na ratio (orange diamonds), and NH_4^+ (blue circles) for the millennium between 2.0 k and 1.0 k yr B.P. in the B40 record. Close agreement between the BC and NH_4^+ seasonal cycles in B40 indicates a common source and/or transport. Seasonal timing in both Figures 4a and 4b largely was determined from the nssS/Na ratio with the summer maxima in nssS/Na assigned a date of 1 January each year. Confidence intervals show 1σ standard error of the mean.

Five BC standards ranging in concentration from ~0.1 to ~6.0 ng g^{-1} were measured at the beginning and end of each analysis day, with ~1.0 ng g^{-1} quality control standards analyzed every ~2.5 h during routine pauses in the continuous ice core analyses for calibration of the analytical system. Standards were made from sequential dilutions of Cabojet 200. Repeatability of the DRI method is demonstrated by close correspondence in replicate measurements of a 6 m section of the B40 core (Figure S1). Parallel samples were analyzed on three different days in September and October, 2013. Small differences in concentration between parallel longitudinal samples result from glaciological noise in snow deposition [*Mosley-Thompson et al.*, 2001]. Slight offsets in depth, typically $<$0.01 m, also may occur from offset depth registration between parallel measurements (Figure S1). Subannually resolved measurements are highly repeatable (Figure S1), and BC concentration and flux uncertainties in the ice core records are estimated to be $<$5%.

Ammonium was measured using continuous flow methods [*Kaufmann et al.*, 2008; *Pasteris et al.*, 2014b]. Standards that bracketed the sample concentrations were analyzed at the beginning and end of the analysis day. Quality control standards also were analyzed every ~2.5 h during routine pauses in the continuous ice core analyses for calibration of the analytical system.

2.3. Modeling

To examine the role of insolation on Southern Hemisphere BB, we analyzed climate model outputs from the National Center for Atmospheric Research Community Climate System Model version 4 (CCSM4) for two time periods: the preindustrial and the mid-Holocene (6 k yr B.P.). The fully coupled general circulation model, CCSM4, consisted of atmosphere, ocean, land, and sea ice components that were linked through a coupler that exchanges state information and fluxes between the components [*Gent et al.*, 2011]. The atmospheric model was the Community Atmosphere Model version 4 (CAM4), which used the Lin-Rood finite volume core with a 1.25° × 0.9° uniform resolution, and 26 levels in the vertical [*Neale et al.*, 2013]. The land model, the Community Land Model version 4 (CLM4), used the same horizontal resolution as CAM4. The ocean model component used the Parallel Ocean Program version 2 [*Smith et al.*, 2010] with 60 vertical levels. The horizontal resolution was uniform at 1.11°, while the meridional resolution ranges from 0.27° at the equator to 0.54° at 33°N/S and was constant at higher latitudes. The sea ice component used the same horizontal grid as the ocean component and included the impact of BC in the radiation physics.

The land model component, CLM4, contained a prognostic fire algorithm that depended on fuel availability and near-surface soil moisture conditions and was based on *Thonicke et al.* [2001], with a modification to simulate fire seasonality [*Oleson et al.*, 2010]. Climate and weather conditions, and vegetation composition

and structure, all contributed to fires; however, human-changed fire regimes were not considered in this model. Fire-induced vegetation mortality resulted in an adjustment in the carbon and nitrogen pools. Fuel availability depended on the aboveground biomass and fuel combustibility depended on relative humidity, surface soil wetness, and surface air temperature. More details can be found in *Oleson et al.* [2010] and *Thonicke et al.* [2001].

We analyzed the 1850 C.E. preindustrial [*Gent et al.*, 2011] and 6 k yr simulations, which followed the Coupled Model Intercomparison Project phase 5 and Paleoclimate Modeling Intercomparison Project phase 3 (PMIP3) protocols, respectively. In the preindustrial run, the incoming solar radiation at the top of atmosphere was set to a constant 1360.9 W m^{-2}, and CO_2 was fixed at 284.7 parts per million (ppm). Aerosol concentrations were prescribed and non–time varying with the same spatial distribution based on a historical simulation using the chemistry component of CCSM4, which used prescribed historical emissions [*Lamarque et al.*, 2010]. In accordance with the PMIP3 experimental design, orbital parameters were set to 6 k yr B.P. values (eccentricity = 0.018682, obliquity = 24.105°, and angular precession (°) = 0.87°), while aerosols, the solar constant, ice sheets, topography, and vegetation were fixed at preindustrial values. The concentration of CO_2 was reduced to 280 ppm. Although the vegetation distribution was fixed, both experiments were run with a carbon-nitrogen biogeochemical model, which allowed for prognostic changes in vegetation phenology [*Lawrence et al.*, 2011]. Accordingly, the leaf area index and vegetation height were prognostic and affected by climate [*Thornton et al.*, 2007]. The fully coupled preindustrial control simulation was run for 1300 years. The 6 k yr simulation was branched from the preindustrial simulation at model year 800 and run for an additional 500 years. We computed annual and seasonal means based on 156 years of data from each simulation, corresponding to model years 953–1108, which are available on the earthsystemgrid.org. Calculating the annual and seasonal means based on 500 years of the preindustrial simulation (model years 800–1300) did not change our results. The statistical significance of the anomalies (6 k yr—preindustrial) was assessed using a Student's *t* test with the null hypothesis that the sample means are from the same population.

2.4. Tropical Illimani Ice Core

The original age model from *Kellerhals et al.* [2010] for the Illimani ice core was developed through reference horizons from nuclear bomb tests and volcanic tie points as well as ^{14}C dating. We shifted the published Illimani age model by 50 years from 1595 to 565 yr B.P., linearly between 50 years and 0 years from 565 to 145 yr B.P., and then by 0 years from 145 yr B.P. to the top of the record. These adjustments were well within the uncertainties in the underlying data used for dating [*Kellerhals et al.*, 2010] and demonstrate overall agreement with the Antarctic B40 BC record.

2.5. Charcoal Composite Records

Charcoal records from South America were acquired, transformed, and compiled from the Global Charcoal Database using the *Blarquez et al.* [2014] paleofire R script from four regions in South America (Figure 1). Data first were transformed utilizing the pfTransform routine, and the composite records were smoothed using the pfCompositeLF routine [*Blarquez et al.*, 2014]. This method utilized 20 year, nonoverlapping bins and a LOWESS smoother with a 200 year half-width window from 2500 to 0 yr B.P. Confidence interval calculations are described in *Blarquez et al.* [2014] and calculated with 1000 repetitions. Details about the compiled charcoal records are provided in the supporting information Tables S1–S4.

3. Results

3.1. Mid-Holocene

BC fluxes in the WD Holocene record (50 year averages) more than doubled from <25 μg m^{-2} yr^{-1} at the end of the last glacial termination (14 k yr B.P.) to >50 μg m^{-2} yr^{-1} in the mid-Holocene (~8 to 6 k yr B.P.). Since this mid-Holocene peak, although the data in this section are sparse, the BC declined to <30 μg m^{-2} yr^{-1} in the recent past (Figure 2). The most pronounced increase at ~11 k yr B.P. was the result of a large increase in the water accumulation rate at that time rather than significant changes in BC concentrations in the ice (Figure 2).

Overall changes in BC flux during the Holocene closely paralleled austral spring (October [burning season]) minus late summer (February [growing season]) insolation at 15°S, which varied by more than 45 W m^{-2} [*Laskar et al.*, 2004] (Figure 5e). During the mid-Holocene, the difference between fire season insolation

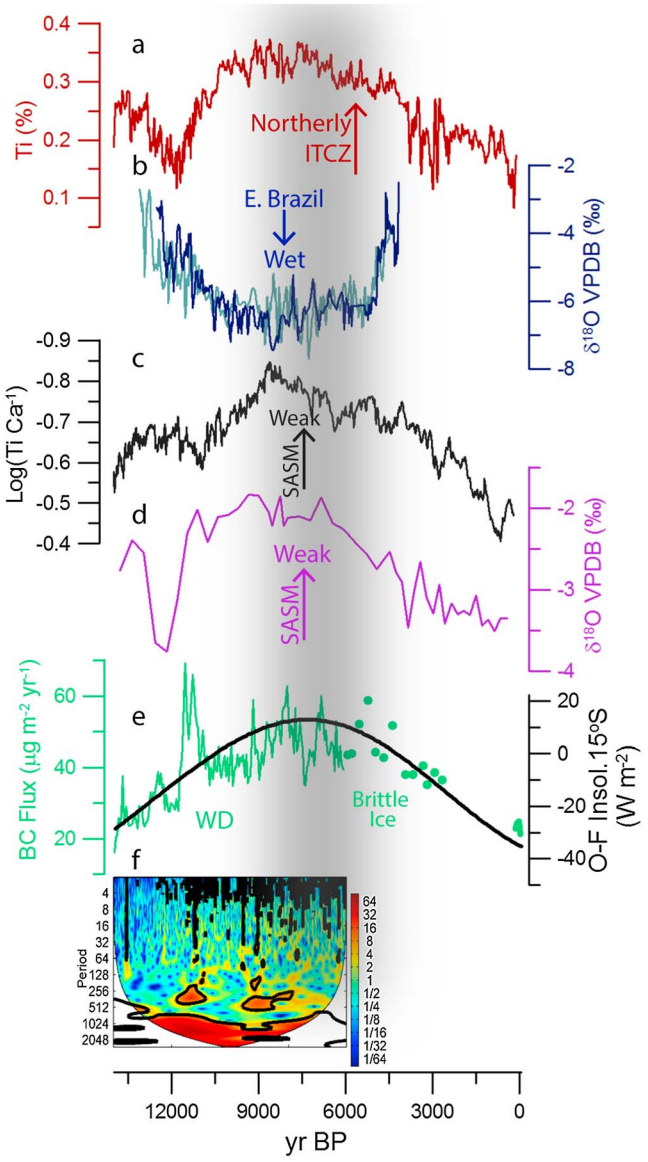

Figure 5. The 14,000 years of BC flux from WD compared to low- and middle-latitude records. (a) Cariaco Basin sediment core (10-point average) [*Haug et al.*, 2001]. (b) $\delta^{18}O$ of stalagmite carbonate in RN-1 (dark blue) and RN-4 (light blue) from Rio Grande do Norte Cave (three-point average) [*Cruz et al.*, 2009]. (c) Gulf of Guayaquil marine sediment core (M772-059) Ti/Ca (three-point average, axis reversed) [*Mollier-Vogel et al.*, 2013]. (d) $\delta^{18}O$ of stalagmite carbonate from Botuvera Cave (BTV-3a) [*Wang et al.*, 2007]. (e) October (burn season) minus February (growing season) insolation [*Laskar et al.*, 2004] for 15°S (black) and 50 year averages of BC flux from WD (green, dots indicate the brittle ice zone) with the BC flux for the past 150 years from *Bisiaux et al.* [2012b]. (f) Continuous wavelet power spectrum of the 1 year averaged WD BC flux from 14.0 k yr B.P. to ~6.1 k yr B.P. Thick black contour represents the 5% significance level against red noise and the cone of influence where edge effects may distort the analysis [*Grinsted et al.*, 2004], demonstrating significant coherence at 3 to 7 years and ~1000 to ~2000 years. Gray bar identifies increased BC flux in WD.

and growing season insolation increased. We chose to compare the burning season to growing season insolation because insolation during these seasons may impact biomass growth and subsequent burning. Insolation-driven model experiments simulate a positive carbon loss due to fires anomaly (6 k yr minus preindustrial) for September–November (SON) for three SA regions: eastern Amazonia, a second region approximately corresponding to the modern Pampas, and southeastern Colombia (Figure 6a). The simulations suggest that increased carbon loss due to fires was associated with a relative decrease in SON precipitation (Figure 6b), SON soil moisture (Figure 6c), and annual precipitation (Figure S2a), as well as increases in annual fire season length (Figure 6d) and SON temperature (Figure S2c). The carbon loss due to fires from the model simulations for the three SA regions ranged between ~40 to 80 gC m^{-2} yr^{-1} for the eastern Amazonia region, ~40 gC m^{-2} yr^{-1} for the Pampas region, and ~80 to 120 gC m^{-2} yr^{-1} for the southeastern Colombia region for the 6 k yr simulation (Figure S3a). The preindustrial carbon loss due to fires model results demonstrated a decrease to ~0 to 20 gC m^{-2} yr^{-1} for eastern Amazonia and the Pampas region, and ~40 to 80 gC m^{-2} yr^{-1} for southeastern Colombia (Figure S3b). While the carbon loss due to fires simulated in the model includes all forms of carbon (black, brown, and organic carbon), the magnitude of modeled change from 6 k yr to preindustrial is similar to the observed change in the WD BC flux from 6 k yr to preindustrial.

3.2. Little Ice Age

Variations in Antarctic BC flux also were recorded during the past 2500 years in the east Antarctic B40 ice core. While similar sources potentially were driving BC flux records both at WD and B40, we present the two records separately because of minimal temporal overlap between the two records and differences in location. Beginning at 2500 yr

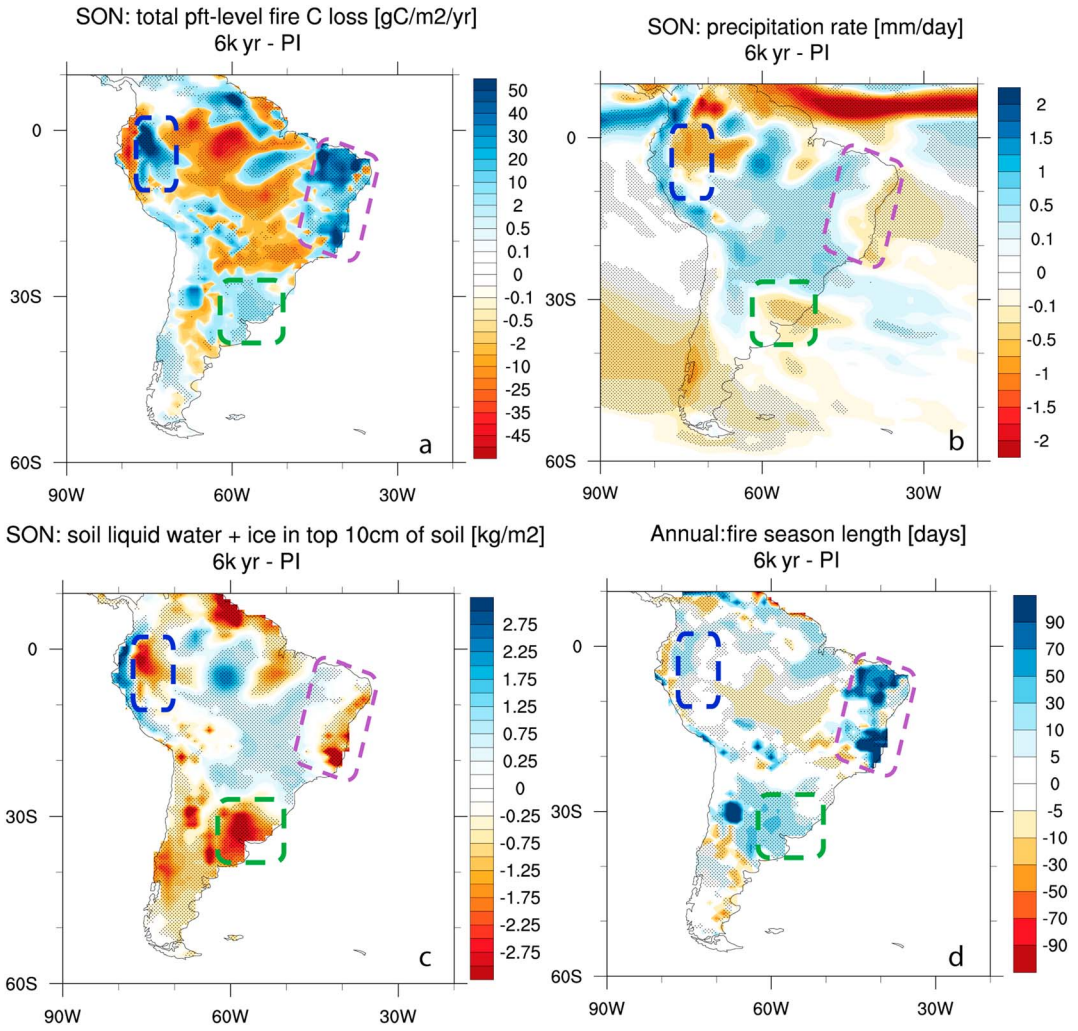

Figure 6. The 6 k yr minus preindustrial (PI) anomalies from CESM1 insolation-driven model simulations. (a) SON total carbon loss due to fires; (b) SON precipitation rate; (c) SON soil liquid water and ice in the top 10 cm of soil; and (d) annual mean fire season length. Purple dashed box indicates the eastern Amazonia region, the green dashed box indicates the Pampas region, and the blue dashed box represents the southeastern Colombia region. All regions demonstrate an anomalous increase in carbon loss due to fire. Anomalies that are statistically significant above the 95% confidence level are stippled.

B.P., BC fluxes gradually increased from ~20 μg m^{-2} yr^{-1} to ~30 μg m^{-2} yr^{-1} by 595 yr B.P. This gradual rise was followed by a sharp decline to 10 μg m^{-2} yr^{-1} by 500 yr B.P. Low levels persisted until ~200 yr B.P., followed by a gradual increase to present levels of approximately 15 μg m^{-2} yr^{-1} (Figure 3). BC fluxes at WD were approximately 1.5 times greater than B40 fluxes during the recent past. This is driven in part by the lower accumulation at B40 (Table 1), resulting in overall lower BC fluxes. Further discussion of the BC flux differences in Antarctica is presented in section 4.2.

In addition to BC, NH_4^+ has often been used as surrogate of BC in ice. Ammonium has been used successfully in ice cores from Greenland as a BB proxy [*Fischer et al.*, 2015; *Legrand et al.*, 1992]. For Antarctica, *Pasteris et al.* [2014b] suggested that NH_4^+can serve as a BB proxy. However, previous studies also have suggested that marine zooplankton may be a source of NH_4^+ for Antarctica [*Kaufmann et al.*, 2010]. Though more moderate than changes in BC flux over the last 2500 years, the B40 NH_4^+ flux record followed a similar pattern with fluxes increasing from 2500 yr B.P. to a peak of ~80 μg m^{-2} yr^{-1} in ~570 yr B.P., followed by a sharp decline to ~45 μg m^{-2} yr^{-1} by ~500 yr B.P., exactly coincident with the decline in BC flux (Figure 3). The decline in NH_4^+ flux was followed by rapid and significant increase during the past ~100 years. This period of

decreased BC and NH_4^+ flux at ~500 yr B.P. is coincident with the LIA, a period of significant changes in low- to middle-latitude hydroclimate, which will be described in section 4.4.

4. Discussion

BC and other BB emissions—such as organic carbon aerosols, carbon monoxide (CO), and methane (CH_4)—increasingly are recognized as major components of climate forcing [*Bond et al.*, 2013; *Jones et al.*, 2007; *Shindell and Faluvegi*, 2009]. Accurate model simulations of past and future climate critically depend on detailed understanding of the natural variations and climate drivers of BB emissions as well as their impact on atmospheric aerosol and gas concentrations.

4.1. Source of BC

BB tracers deposited in Antarctica must be transported across the Southern Ocean from low- to middle-latitude source regions so the distal B40 and WD ice core records reflect both changes in BB emissions and possible changes in long-range atmospheric transport. In order to constrain the source of BC to Antarctica over the Holocene, we compared the following: (1) seasonal timing in BC deposition in Antarctica, (2) current Southern Hemisphere BC observations and BC sources to Antarctica, (3) model simulations from 6 k yr, and (4) proximal climate and BB records from the low to middle latitudes.

BC concentration from the WD ice core and BC and NH_4^+ concentration from the B40 ice core were greatest for the austral spring season (Figure 4). The modern peak in tropical and extratropical SA burning occurs during the austral spring from August to October, and the monsoonal rainfall maximum occurs during the austral summer from December to February [*Fiebig et al.*, 2009; *Koch et al.*, 2007] (Figure S4). Similarly, southern Africa burning season occurs from July to September [*Mieville et al.*, 2010] with the exception of the south-western fynbos vegetation type which burns from December to February [*Archibald et al.*, 2010; *Daniau et al.*, 2013]. In Northern Australia, the burning season is from May to October with a peak in September [*Koch et al.*, 2007]. From the seasonal cycle results, both WD and B40 potentially are sourced by BB in South America, Australia, or Africa.

Model simulations show that the carbonaceous load in Antarctica is dominated by SA BB [*Koch et al.*, 2007]. This is supported further by observations from the Antarctic Peninsula [*Pereira et al.*, 2006], East Antarctica [*Weller et al.*, 2013; *Wolff and Cachier*, 1998], and the South Pole [*Bodhaine*, 1995] as well as air mass back trajectory analyses [*Fiebig et al.*, 2009; *Hara et al.*, 2010]. Using a year of atmospheric aerosol BC measurements from the Troll Research Station in eastern Antarctica and back trajectory analyses, *Fiebig et al.* [2009] identified Central Brazil as the predominate source of BC to eastern Antarctica. *Hara et al.* [2010] suggested that BC at Syowa Station was sourced from both SA and southern Africa; however, we note that Syowa Station is located much farther east than B40, while Troll Station is relatively close.

From the mid-Holocene and preindustrial model-simulated results, a significant increase in the annual fire season length and SON carbon loss due to fires was observed for SA and Northern Australia (Figures S2 and S3). For the latter, statistically significant grid cells for annual fire season length and carbon loss due to fires are limited to a small region at ~15°S (Figures S2 and S3). Carbon loss due to fires in Northern Australia ranged from ~40 to 60 gC m^{-2} yr^{-1} for the 6 k yr simulation and from ~0 to 20 gC m^{-2} yr^{-1} in the preindustrial (Figure S3) similar to the observations of BC flux in the WD ice core. However, the model simulations also show less precipitation during the wet season for Northern Australia which would have reduced biomass growth (Figure S2b) and potentially limited fuel production which is a critical component of the fire cycle in Northern Australia [*Olson et al.*, 1999; *van der Werf et al.*, 2008]. Considering these results and the results from modern observations, we primarily focus on SA as the source of BC to Antarctica.

Within SA, model results demonstrate three potential regions of increased BB during the mid-Holocene (Figure 6). Proximal charcoal records suggest marked regional differences in burning during the last 2500 years within SA (Figures 7f and S5, Tables S1–S4). Charcoal compilations for the eastern Amazonia, western Amazonia, and Pampas regions, as indicated by the model experiments, were compared to Patagonia charcoal compilations. Charcoal compilations from western Amazonia and Patagonia show only minor variations during the past 2500 years (Figure 7f). Although comprised of only five sites, the Pampas compilation indicates a decline from ~2000 to ~900 yr B.P. followed by a rapid increase (Figure 7f). The eastern Amazonia compilation more closely resembles BC deposited at the B40 ice core site, with a decline beginning at ~800 yr

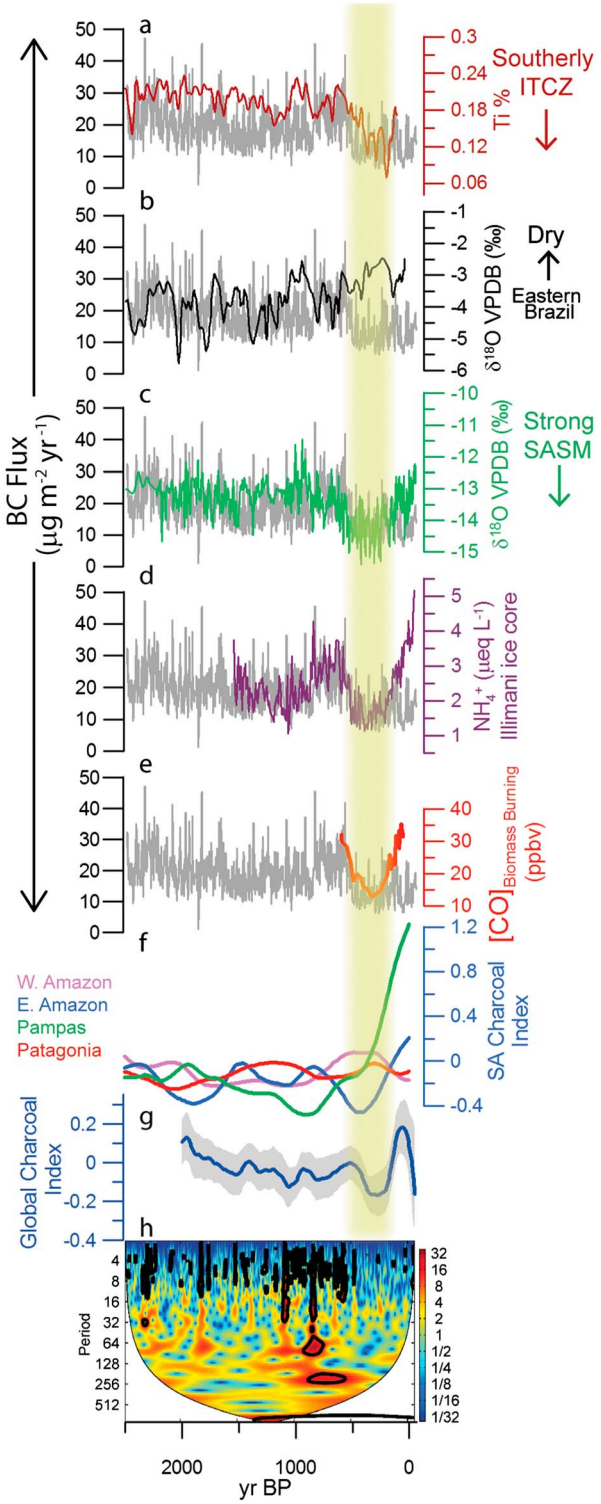

B.P. and reaching a minimum during the LIA, followed by an increase to the present (Figure 7f). The eastern Amazonia charcoal results are also broadly consistent with the proximal Illimani ice core record. The Illimani ice core record of NH_4^+ spanning the last 1500 years from the tropical Bolivian Andes (Figure 7d, location shown in Figure 1) is a proximal ice core record originally interpreted primarily as a proxy of Amazonian temperature [*Eichler et al.*, 2009; *Kellerhals et al.*, 2010] rather than more traditionally as a proxy of biomass burning [*Legrand et al.*, 2016]. Given the decadal-to-century scale agreement with the BC and NH_4^+ records from the B40 ice core, we suggest that the Illimani ice core NH_4^+ record also reflects a reduction in BB during the LIA (Figure 7). These observations further support that the Antarctic ice core BB records primarily reflect SA BB emissions with little modification from changes in long-range transport during the relatively stable climate of the Holocene.

4.2. Long-Range Transport

The close agreement between model simulations and proximal records further supports the interpretation of the ice core BC records as proxies of regional-scale BB emissions not significantly

Figure 7. Recent B40 BC flux in gray as a 7 year median compared to low- and middle-latitude records. (a) Cariaco Basin sediment core (five-point average) [*Haug et al.*, 2001]. (b) Stalagmite $\delta^{18}O$ from Diva Cave (DV2) (five-point average) [*Novello et al.*, 2012]. (c) Laguna Pumacocha $\delta^{18}O$ from authigenic lake calcite (three-point average) [*Bird et al.*, 2011]. (d) Tropical SA (Illimani) ice core NH_4^+ [*Kellerhals et al.*, 2010] with scaled age model. (e) BB component of CO from the South Pole [*Wang et al.*, 2010]. (f) Transformed charcoal indices from the Global Charcoal Database (errors are shown in Figure S5). (g) Z scores of transformed global charcoal influx with 95% confidence interval (gray) [*Marlon et al.*, 2008]. (h) Continuous wavelet power spectrum of the 1 year averaged B40 BC flux, demonstrating significant coherence at 3 to 7 years. Yellow bar indicates the approximate timing of decreased BC flux in B40.

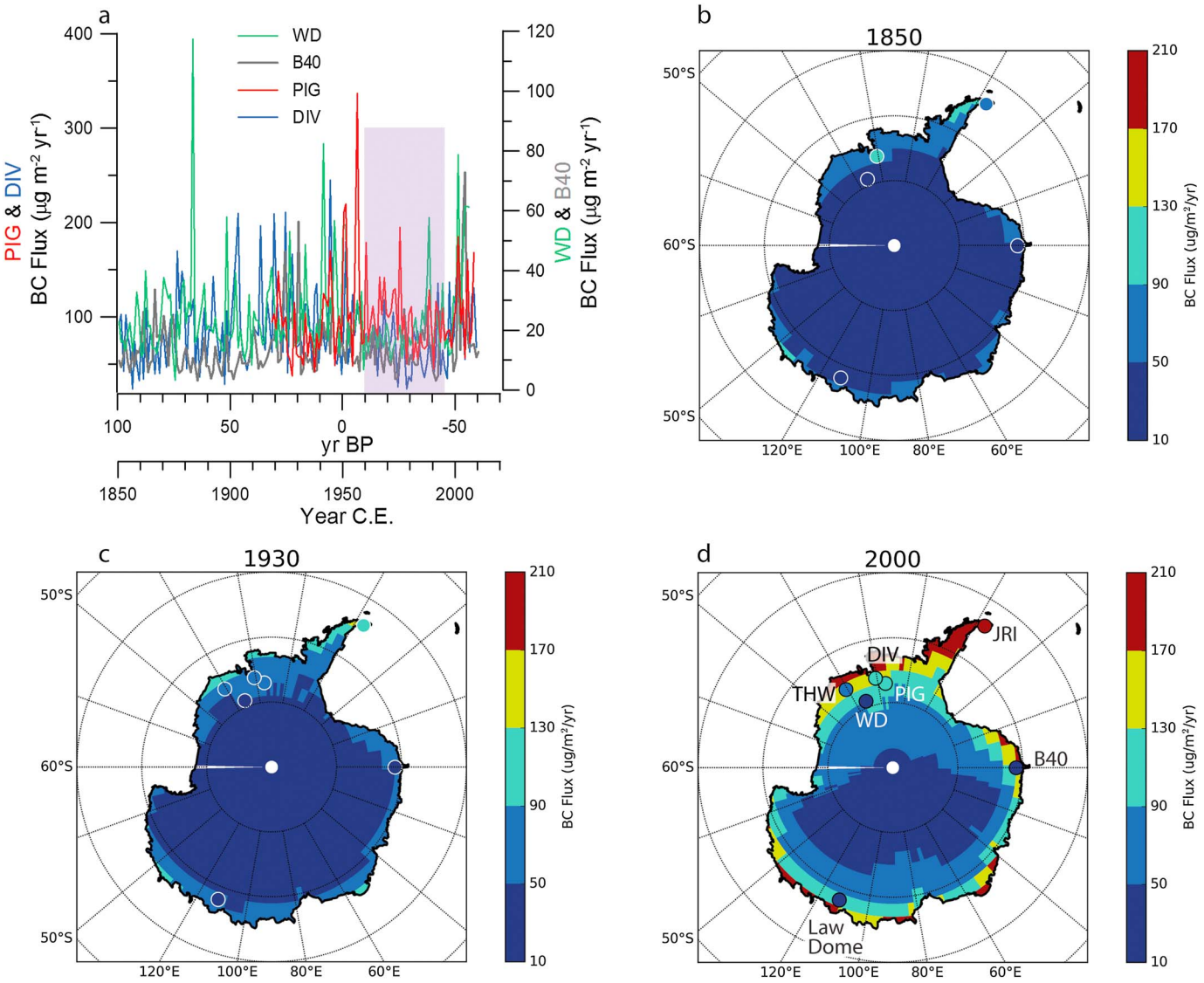

Figure 8. Recent Antarctic BC fluxes. (a) Annual averaged B40 BC flux in gray and WD from *Bisiaux et al.* [2012b] in green plotted on the right axis. Annual averaged BC flux for PIG and DIV, plotted on the left axis. Purple bar highlights the period of reduced BC flux. (b–d) BC flux model results (shown in μg m^{-2} yr^{-1}) from *Lee et al.* [2013] for three time periods compared to BC flux data from the seven ice cores. Ice core data represent a 5 year average centered on the modeled year. Model results generally agree with measurements.

impacted by changes in long-range transport. From the analysis of two Antarctic ice cores, *Bisiaux et al.* [2012b] demonstrated that Southern Hemisphere rainfall variability was the primary factor influencing low- to middle-latitude BC source emissions, rather than transport on decadal to subdecadal timescales during the past 150 years. Here we compared the past 150 years of BC for a suite of ice cores from Antarctica (Figures 8 and S6, Table 1), and we evaluated the measured fluxes against modeled BC flux [*Lee et al.*, 2013] to investigate temporal and spatial variations in BC fluxes. We compared the East Antarctic Law Dome record [*Bisiaux et al.*, 2012a, 2012b], the West Antarctic Pine Island Glacier (PIG), Thwaites Glacier (THW) and the divide between Pine Island and Thwaites Glaciers (DIV) [*Criscitiello et al.*, 2014] records, and the James Ross Island (JRI) record from the Antarctic Peninsula [*Mulvaney et al.*, 2012; *Arienzo et al.*, 2016].

Figure 8a shows BC fluxes for four ice cores. The other three records are plotted in Figure S6 for comparison. Overall, good agreement is observed on the decadal scale from 1925 C.E. to present with the ice cores demonstrating increased BC flux variability in the early to middle 1900s and a reduction in BC flux from

approximately 1960 to the mid-1990s. This was followed by an increase since the mid-1990s for most ice cores (Figures 8a and S6). The measured ice cores also agree well with modeled BC flux from *Lee et al.* [2013] particularly for the 1850 and 1930 C.E. time periods (Figures 8b–8d). Overall, the ice cores and model demonstrate increased BC flux from early industrialization to present throughout Antarctica; however, modeled BC fluxes are too high for eastern Antarctica for the year 2000 C.E. (Figure 8d).

While BC flux trends between these cores agree over the past 150 years, there are differences in the overall magnitude of BC flux. For example, WD, B40, and Law Dome showed lower BC fluxes than PIG, DIV, THW, and JRI sites (Figure S6), which is also reflected in the modeled BC flux results. BC has been shown to be primarily deposited through wet deposition [*Flanner et al*., 2007] and therefore is scavenged along the higher accumulation coastal regions with lower BC fluxes inland as accumulation rates decrease. This is reflected in the ice core BC flux results, with lower BC flux in areas which have lower accumulation and areas which are farther from the coast.

Similarities in BC flux trends in the ice core array for the last 150 years suggest that BC generally is well mixed in the Antarctic atmosphere, implying that the longer ice core records are potentially representative of BC deposition for Antarctica and likely reflect variations in the Southern Hemisphere BB emissions rather than changes in long-range atmospheric transport. Similar observations have been made in Antarctica for industrial lead, which also must be transported long distances from middle- and low-latitude source regions to Antarctica across the Southern Ocean [*McConnell et al*., 2014].

4.3. Linkages to Low-Latitude Hydroclimate During the Mid-Holocene

Middle- and low-latitude paleoclimate records and model simulations link insolation variations during the Holocene to the position of the Intertropical Convergence Zone (ITCZ) and SA tropical precipitation patterns [*Clement et al*., 2004; *Haug et al*., 2001]. The WD ice core BC record spanning the last 14 k years showed that long-term BC fluxes were highest during the mid-Holocene when the ITCZ was shifted north (Figure 5a). The ITCZ modulates moisture flux to the SA Summer Monsoon (SASM) region [*Bird et al*., 2011; *Vuille et al*., 2012], and Amazon Basin precipitation patterns primarily are determined by the strength of the SASM [*Vuille et al*., 2012]. Mid-Holocene changes in the SASM reflected in paleoclimate proxies show decreased precipitation in western [*Mollier-Vogel et al*., 2013] and southern Amazonia [*Wang et al*., 2007] (Figures 5c and 5d) and increased precipitation in eastern coastal Brazil [*Cheng et al*., 2013; *Cruz et al*., 2009] (Figure 5b), consistent with a weaker SASM when the ITCZ was shifted north. This antiphased SA precipitation pattern is termed the SA Precipitation Dipole [*Cheng et al*., 2013] and is observed in the modeled precipitation results for December–February (DJF) (Figure S2b). We postulate that the mid-Holocene period of reduced SASM—driven by insolation and the position of the ITCZ—resulted in an increase in BB in eastern Amazonia and the Pampas region and the higher BC fluxes observed in the WD record (Figures 5 and 6).

Insolation-burning relationships also have been observed over longer timescales in southern Africa grasslands, where increased austral summer insolation, a southerly ITCZ, and an increase in precipitation amount were shown to increase savanna BB due to an associated increase in grassland biomass [*Daniau et al*., 2013]. However, in SA during the mid-Holocene, pollen records suggest that vegetation changes were not a significant driver of the variations in SA burning. Lake and marine sediment pollen records from eastern Amazonia indicate that vegetation during the LGM was similar to today (vegetation dominated by caatinga, cerrado, and dry forest), with possibly drier and cooler conditions [*Mayle et al*., 2009]. In the Pampas region, pollen records suggest that the LGM was a period of aridity, with overall similar vegetation, while the early Holocene was wetter in some regions [*Mancini et al*., 2005; *Piovano et al*., 2009].

While the records of BB from Antarctica follow low-latitude hydroclimate changes, there are discrepancies with published charcoal records. Charcoal compilations from the American tropics and monsoonal Australia showed little change during the early to mid-Holocene [*Marlon et al*., 2013] (Figure S7), as do compilations of the southern tropics (0–30°S) and southern extratropics (30°S–90°S) [*Daniau et al*., 2012] (Figure S7), and central and South America [*Power et al*., 2008]. The mid-Holocene model simulations (Figure 6) suggest significant spatial variations in BB throughout SA, which may be lost when compiling charcoal records over large regions. Additionally, longer charcoal records extending into the mid-Holocene are necessary to determine regional-scale differences (Tables S1–S4).

4.4. Linkages to Low-Latitude Hydroclimate During the LIA

Similar connections between the position of the ITCZ, low-latitude SA hydroclimate, and BB also were observed during the LIA. Sharp declines in BC and NH_4^+ fluxes at the onset of the LIA ~600 yr B.P. and low concentrations from ~500 to ~250 yr B.P. observed in the B40 ice core are consistent with markedly lower BB in the SA source regions (Figures 7d and 7f). Low- and middle-latitude SA climate proxies suggest that the ITCZ shifted southward over the Atlantic [*Haug et al.*, 2001] (Figure 7a) and Pacific [*Sachs et al.*, 2009] during the LIA, resulting in an enhanced SASM [*Vuille et al.*, 2012]. Consistent with precipitation patterns during the mid-Holocene, the Laguna Pumacocha [*Bird et al.*, 2011] (Figure 7c) and western Amazonia cave calcite records [*Kanner et al.*, 2013; *Vuille et al.*, 2012] indicate strengthened SASM, while speleothem records from farther east show decreased precipitation [*Novello et al.*, 2012] (Figure 7b). The sharp decline in BC and NH_4^+ in the B40 record from 565 to 500 yr B.P., as well as low levels from 500 to ~250 yr B.P., also coincided with a reduction in Southern Hemisphere BB emissions indicated by isotope ratios in CO measured in an ice core from South Pole [*Wang et al.*, 2010] (Figure 7e) and by worldwide [*Marlon et al.*, 2008] (Figure 7g) and Southern Hemisphere [*Marlon et al.*, 2016] compilations of charcoal records during the LIA. Therefore, during the LIA the eastern Amazonia region may have been wetter during the SA fire season because of a strengthened SASM, thereby reducing fire potential. Agreement of the ice core BC and NH_4^+ fluxes with proxy climate data is not as robust during the past ~250 years, possibly because of anthropogenic changes in BB and fossil fuel emissions.

Similar to the observations from the mid-Holocene, little change is observed in charcoal compilations for the LIA from the tropics (30°N to 20°S) and from the southern extratropics (>20°S) [*Marlon et al.*, 2008]. However, when comparing charcoal records from various regions within SA (Figure 7f) we observe marked differences, suggesting the heterogeneous fire response is not captured when compiling charcoal records over large regions.

4.5. Linkages to ENSO

The SASM is the major driver of precipitation to SA, but the El Niño–Southern Oscillation (ENSO) also influences precipitation variability in the region [*Cheng et al.*, 2013; *Vuille et al.*, 2012]. El Niño events form during periods of reduced equatorial easterlies and typically result in less than normal precipitation in tropical SA, with more humid conditions in the midlatitudes that potentially influence BB [*Cheng et al.*, 2013; *Vuille et al.*, 2012]. Spectral analysis of the continuous WD annual BC flux time series from 14 k yr B.P. to ~6.1 k yr B.P. demonstrated an absence of variance in the ENSO band (3–7 year periodicity) from 14 k yr B.P. to 11.5 k yr B.P. and then persistent ENSO-like periodicity from ~11.5 k yr B.P. to the end of the continuous WD record ~6.1 k yr B.P. (Figures 5f, S8). In general, higher BC concentrations and fluxes were associated with ENSO-like variability during the Holocene WD record. In the B40 ice core, reduced ENSO frequencies were observed during periods of lower BC concentrations, particularly during the LIA (Figure 7h). A SA ENSO proxy [*Moy et al.*, 2002] shows ENSO frequency increased after ~7 k yr B.P. with a peak between ~5 k yr B.P. to 1.2 k yr B.P. and a reduced ENSO frequency during the LIA.

5. Conclusion: Insights Into Past and Future Climate-Fire Linkages

BC deposition to Antarctica has increased since industrialization with predicted continued increase in BC emissions from source areas [*Bond et al.*, 2013]. The detailed, long-term records of Antarctic BC and other BB indicators, together with the model simulations, provide a basis for understanding natural climate-fire relationships in the Southern Hemisphere. Understanding BC emissions in the Southern Hemisphere is of interest due to its important role in climate forcing and potential impacts to ice sheet albedo [*Bond et al.*, 2013]. Utilizing both ice core records and climate model simulations, we attribute Antarctic BC flux variations and hence SA BB throughout the Holocene to seasonal insolation changes and related low-latitude hydroclimate variations during the mid-Holocene, specifically the following: (1) increased BB emissions from >45 W m^{-2} relative changes in relative burning and growing season insolation in the low-latitude Southern Hemisphere and (2) precipitation-driven increases in BB emissions in SA arising from an insolation-driven northerly shift in the ITCZ and subsequent weakening of the SASM in the mid-Holocene. During the LIA, the opposite occurred with climate proxies indicating a southerly shift in the ITCZ and subsequent strengthening of the SASM that coincided with the lowest rates of BC deposition observed in Antarctic ice during the Holocene.

This study demonstrates the importance of low-latitude precipitation on biomass burning and hence export of BC to Antarctica in the past. However, future precipitation predictions under increased greenhouse gas emissions remain uncertain for the low latitudes. Recent model experiments demonstrate that under higher emission scenarios, the Southern Hemisphere tropical regions, including SA, will experience substantial regional-scale changes in rainfall amount [*Chadwick et al.*, 2015]. Our findings that hydroclimate conditions in South America modulated biomass burning and preanthropogenic Antarctic BC throughout the Holocene are important constraints for climate model evaluation and predictions of future BC emissions, deposition to Antarctica and related feedbacks under a warming climate.

Acknowledgments

This work primarily was supported by U.S. National Science Foundation (NSF) grants 0839093, 1142166, 0968391, and 1304540. The acquisition and analyses of the PIG, DIV, and THW cores was supported by NSF OPP ANT-0632031 and NASA NNX10AP09G. B40 ice core samples were supplied by the Alfred-Wegener-Institut. The authors appreciate support of the WAIS Divide Science Coordination Office for the collection and distribution of the WAIS Divide ice core; Ice Drilling and Design and Operations for drilling; the National Ice Core Laboratory for curating the core; Raytheon Polar Services for logistics support in Antarctica; and the 109th New York Air National Guard for airlift in Antarctica. The authors thank L. Layman, O. Maselli, D. Pasteris, and M. Sigl for assistance with BC and other measurements. We also thank R. Kreidberg for his editorial advice and A. Clement for insightful discussions. We would like to thank M. Legrand and two additional anonymous reviewers for their comments which greatly strengthened the manuscript. Charcoal data were obtained from the global charcoal database, and we acknowledge contributions by the paleofire community. BC data for WD and BC and NH_4 data for B40 are accessible at http://www.usap-dc.org/.

References

Archibald, S., R. J. Scholes, D. P. Roy, G. Roberts, and L. Boschetti (2010), Southern African fire regimes as revealed by remote sensing, *Int. J. Wildland Fire*, *19*(7), 861–878.

Arienzo, M., et al. (2016), A method for continuous ^{239}Pu determinations in Arctic and Antarctic ice cores, *Environ. Sci. Technol.*, *50*(13), 7066–7073, doi:10.1021/acs.est.6b01108.

Banta, J., J. McConnell, M. Frey, R. Bales, and K. Taylor (2008), Spatial and temporal variability in snow accumulation at the West Antarctic Ice Sheet Divide over recent centuries, *J. Geophys. Res.*, *113*, D23102, doi:10.1029/2008JD010235.

Bird, B., M. Abbott, M. Vuille, D. Rodbell, N. Stansell, and M. Rosenmeier (2011), A 2,300-year-long annually resolved record of the South American summer monsoon from the Peruvian Andes, *Proc. Natl. Acad. Sci. U.S.A.*, *108*(21), 8583–8588, doi:10.1073/pnas.1003719108.

Bisiaux, M., R. Edwards, J. McConnell, M. Albert, H. Anschutz, T. Neumann, E. Isaksson, and J. Penner (2012a), Variability of black carbon deposition to the East Antarctic Plateau, 1800–2000 AD, *Atmos. Chem. Phys.*, *12*(8), 3799–3808, doi:10.5194/acp-12-3799-2012.

Bisiaux, M., R. Edwards, J. R. McConnell, M. A. J. Curran, T. D. Van Ommen, A. M. Smith, T. A. Neumann, D. R. Pasteris, J. E. Penner, and K. Taylor (2012b), Changes in black carbon deposition to Antarctica from two high-resolution ice core records, 1850–2000 AD, *Atmos. Chem. Phys.*, *12*(9), 4107–4115, doi:10.5194/acp-12-4107-2012.

Blarquez, O., B. Vanniere, J. Marlon, A. Daniau, M. Power, S. Brewer, and P. Bartlein (2014), paleofire: An R package to analyse sedimentary charcoal records from the Global Charcoal Database to reconstruct past biomass burning, *Comput. Geosci.*, *72*, 255–261, doi:10.1016/j.cageo.2014.07.020.

Bodhaine, B. A. (1995), Aerosol absorption measurement at Barrow, Mauna Loa, and the South Pole, *J. Geophys. Res.*, *100*, 8967–8975.

Bond, T., et al. (2013), Bounding the role of black carbon in the climate system: A scientific assessment, *J. Geophys. Res. Atmos.*, *118*, 5380–5552, doi:10.1002/jgrd.50171.

Buizert, C., et al. (2015), The WAIS Divide deep ice core WD2014 chronology—Part 1: Methane synchronization (68–31 ka BP) and the gas age–ice age difference, *Clim. Past*, *11*(2), 153–173, doi:10.5194/cp-11-153-2015.

Calder, W., D. Parker, C. Stopka, G. Jiménez-Moreno, and B. Shuman (2015), Medieval warming initiated exceptionally large wildfire outbreaks in the Rocky Mountains, *Proc. Natl. Acad. Sci. U.S.A.*, doi:10.1073/pnas.1500796112.

Chadwick, R., P. Good, G. Martin, and D. Rowell (2015), Large rainfall changes consistently projected over substantial areas of tropical land, *Nat. Clim. Change*, doi:10.1038/nclimate2805.

Cheng, H., A. Sinha, F. Cruz, X. Wang, R. Edwards, F. d'Horta, C. Ribas, M. Vuille, L. Stott, and A. Auler (2013), Climate change patterns in Amazonia and biodiversity, *Nat. Commun.*, *4*, doi:10.1038/ncomms2415.

Clement, A., A. Hall, and A. Broccoli (2004), The importance of precessional signals in the tropical climate, *Clim. Dyn.*, *22*(4), 327–341.

Criscitiello, A., S. Das, K. Karnauskas, M. Evans, K. Frey, I. Joughin, E. Steig, J. McConnell, and B. Medley (2014), Tropical Pacific influence on the source and transport of marine aerosols to West Antarctica, *J. Clim.*, *27*(3), 1343–1363, doi:10.1175/jcli-d-13-00148.1.

Cruz, F., M. Vuille, S. Burns, X. Wang, H. Cheng, M. Werner, R. Edwards, I. Karmann, A. Auler, and H. Nguyen (2009), Orbitally driven east-west antiphasing of South American precipitation, *Nat. Geosci.*, *2*(3), 210–214, doi:10.1038/ngeo444.

Daniau, A., et al. (2012), Predictability of biomass burning in response to climate changes, *Global Biogeochem. Cycles*, *26*, GB4007, doi:10.1029/2011GB004249.

Daniau, A., M. Goni, P. Martinez, D. Urrego, V. Bout-Roumazeilles, S. Desprat, and J. Marlon (2013), Orbital-scale climate forcing of grassland burning in southern Africa, *Proc. Natl. Acad. Sci. U.S.A.*, *110*(13), 5069–5073, doi:10.1073/pnas.1214292110.

Eichler, A., S. Brutsch, S. Olivier, T. Papina, and M. Schwikowski (2009), A 750 year ice core record of past biogenic emissions from Siberian boreal forests, *Geophys. Res. Lett.*, *36*, L18813, doi:10.1029/2009GL038807.

Fiebig, M., C. R. Lunder, and A. Stohl (2009), Tracing biomass burning aerosol from South America to Troll Research Station, Antarctica, *Geophys. Res. Lett.*, *36*, L14815, doi:10.1029/2009GL038531.

Fischer, H., S. Schupbach, G. Gfeller, M. Bigler, R. Rothlisberger, T. Erhardt, T. Stocker, R. Mulvaney, and E. Wolff (2015), Millennial changes in North American wildfire and soil activity over the last glacial cycle, *Nat. Geosci.*, *8*(9), 723–727, doi:10.1038/NGEO2495.

Flanner, M. G., C. S. Zender, J. T. Randerson, and P. J. Rasch (2007), Present-day climate forcing and response from black carbon in snow, *J. Geophys. Res.*, *112*, D11202, doi:10.1029/2006JD008003.

Gent, P., et al. (2011), The community climate system model version 4, *J. Clim.*, *24*(19), 4973–4991, doi:10.1175/2011JCLI4083.1.

Grinsted, A., J. Moore, and S. Jevrejeva (2004), Application of the cross wavelet transform and wavelet coherence to geophysical time series, *Nonlinear Processes Geophys.*, *11*(5–6), 561–566.

Hara, K., K. Osada, M. Yabuki, G. Hashida, T. Yamanouchi, M. Hayashi, M. Shiobara, C. Nishita, and M. C. D. Wada (2010), Haze episodes at Syowa Station, coastal Antarctica: Where did they come from?, *J. Geophys. Res.*, *115*, D14205, doi:10.1029/2009JD012582.

Haug, G., K. Hughen, D. Sigman, L. Peterson, and U. Rohl (2001), Southward migration of the intertropical convergence zone through the Holocene, *Science*, *293*(5533), 1304–1308, doi:10.1126/science.1059725.

Jones, A., J. Haywood, and O. Boucher (2007), Aerosol forcing, climate response and climate sensitivity in the Hadley Centre climate model, *J. Geophys. Res.*, *112*, D20211, doi:10.1029/2007JD008688.

Kanner, L., S. Burns, H. Cheng, R. Edwards, and M. Vuille (2013), High-resolution variability of the South American summer monsoon over the last seven millennia: Insights from a speleothem record from the central Peruvian Andes, *Quat. Sci. Rev.*, *75*, 1–10, doi:10.1016/j.quascirev.2013.05.008.

Kaufmann, P., U. Federer, M. Hutterli, M. Bigler, S. Schupbach, U. Ruth, J. Schmitt, and T. Stocker (2008), An improved continuous flow analysis system for high-resolution field measurements on ice cores, *Environ. Sci. Technol.*, *42*(21), 8044–8050, doi:10.1021/es8007722.

Kaufmann, P., F. Fundel, H. Fischer, M. Bigler, U. Ruth, R. Udisti, M. Hansson, M. de Angelis, C. Barbante, and E. W. Wolff (2010), Ammonium and non-sea salt sulfate in the EPICA ice cores as indicator of biological activity in the Southern Ocean, *Quat. Sci. Rev.*, *29*, 313–323.

Keegan, K. M., M. R. Albert, J. R. McConnell, and I. Baker (2014), Climate change and forest fires synergistically drive widespread melt events of the Greenland ice sheet, *Proc. Natl. Acad. Sci. U.S.A.*, *111*(22), 7964–7967.

Kellerhals, T., S. Brutsch, M. Sigl, S. Knusel, H. Gaggeler, and M. Schwikowski (2010), Ammonium concentration in ice cores: A new proxy for regional temperature reconstruction?, *J. Geophys. Res.*, *115*, D16123, doi:10.1029/2009JD012603.

Koch, D., T. Bond, D. Streets, N. Unger, and G. van der Werf (2007), Global impacts of aerosols from particular source regions and sectors, *J. Geophys. Res.*, *112*, D02205, doi:10.1029/2005JD007024.

Lamarque, J., et al. (2010), Historical (1850–2000) gridded anthropogenic and biomass burning emissions of reactive gases and aerosols: Methodology and application, *Atmos. Chem. Phys.*, *10*(15), 7017–7039, doi:10.5194/acp-10-7017-2010.

Laskar, J., P. Robutel, F. Joutel, M. Gastineau, A. Correia, and B. Levrard (2004), A long-term numerical solution for the insolation quantities of the Earth, *Astron. Astrophys.*, *428*(1), 261–285, doi:10.1051/0004-6361:20041335.

Lawrence, D., et al. (2011), Parameterization improvements and functional and structural advances in version 4 of the Community Land Model, *J. Adv. Model. Earth Syst.*, *3*, doi:10.1029/2011MS000045.

Lee, Y. H., et al. (2013), Evaluation of preindustrial to present-day black carbon and its albedo forcing from Atmospheric Chemistry and Climate Model Intercomparison Project (ACCMIP), *Atmos. Chem. Phys.*, *13*(5), 2607–2634, doi:10.5194/acp-13-2607-2013.

Legrand, M., M. De Angelis, T. Staffelbach, A. Neftel, and B. Stauffer (1992), Large perturbations of ammonium and organic acids content in the summit-Greenland Ice Core. Fingerprint from forest fires?, *Geophys. Res. Lett.*, *19*(5), 473–475, doi:10.1029/91GL03121.

Legrand, M., et al. (2016), Boreal fire records in Northern Hemisphere ice cores: A review, *Clim. Past*, *12*, 2033–2059, doi:10.5194/cp-12-2033-2016.

Lim, S., X. Fain, M. Zanatta, J. Cozic, J. Jaffrezo, P. Ginot, and P. Laj (2014), Refractory black carbon mass concentrations in snow and ice: Method evaluation and inter-comparison with elemental carbon measurement, *Atmos. Meas. Tech.*, *7*(10), 3307–3324, doi:10.5194/amt-7-3307-2014.

Mancini, M., M. Paez, A. Prieto, S. Stutz, M. Tonello, and I. Vilanova (2005), Mid-Holocene climatic variability reconstruction from pollen records (32°–52°S Argentina), *Quat. Int.*, *132*, 47–59, doi:10.1016/j.quaint.2004.07.013.

Marlon, J., P. J. Bartlein, A.-L. Daniau, S. P. Harrison, S. Y. Maezumi, M. J. Power, W. Tinner, and B. Vanniére (2013), Global biomass burning: A synthesis and review of Holocene paleofire records and their controls, *Quat. Sci. Rev.*, *65*, 5–25, doi:10.1016/j.quascirev.2012.11.029.

Marlon, J., P. J. Bartlein, C. Carcaillet, D. G. Gavin, S. P. Harrison, P. E. Higuera, F. Joos, M. J. Power, and I. C. Prentice (2008), Climate and human influences on global biomass burning over the past two millennia, *Nat. Geosci.*, *1*(10), 697–702, doi:10.1038/ngeo313.

Marlon, J., et al. (2016), Reconstructions of biomass burning from sediment-charcoal records to improve data–model comparisons, *Biogeosciences*, *13*(11), 3225–3244, doi:10.5194/bg-13-3225-2016.

Mayle, F., M. Burn, M. Power, and D. Urrego (2009), Vegetation and fire at the Last Glacial Maximum in tropical South America, in *Past Climate Variability in South America and Surrounding Regions*, edited by F. Vimeux, F. Sylvestre, and M. Khodri, pp. 89–112, Springer, Netherlands.

McConnell, J., G. Lamorey, S. Lambert, and K. Taylor (2002), Continuous ice-core chemical analyses using inductively coupled plasma mass spectrometry, *Environ. Sci. Technol.*, *36*(1), 7–11, doi:10.1021/es011088z.

McConnell, J., R. Edwards, G. L. Kok, M. G. Flanner, C. S. Zender, E. S. Saltzman, J. R. Banta, D. R. Pasteris, M. M. Carter, and J. D. W. Kahl (2007), 20th-century industrial black carbon emissions altered arctic climate forcing, *Science*, *317*(5843), 1381–1384, doi:10.1126/science.1144856.

McConnell, J., et al. (2014), Antarctic-wide array of high-resolution ice core records reveals pervasive lead pollution began in 1889 and persists today, *Sci. Rep.*, *4*, doi:10.1038/srep05848.

Mieville, A., C. Granier, C. Liousse, B. Guillaume, F. Mouillot, and J.-F. Lamarque (2010), Emissions of gases and particles from biomass burning during the 20th century using satellite data and an historical reconstruction, *Atmos. Environ.*, *44*(11), 1469–1477.

Mollier-Vogel, E., G. Leduc, T. Böschen, P. Martinez, and R. R. Schneider (2013), Rainfall response to orbital and millennial forcing in northern Peru over the last 18 ka, *Quat. Sci. Rev.*, *76*, 29–38, doi:10.1016/j.quascirev.2013.06.021.

Moritz, M., M. Parisien, E. Batllori, M. Krawchuk, J. Van Dorn, D. Ganz, and K. Hayhoe (2012), Climate change and disruptions to global fire activity, *Ecosphere*, *3*(6), 1–22, doi:10.1890/ES11-00345.1.

Mosley-Thompson, E., J. McConnell, R. Bales, P. Lin, K. Steffen, L. Thompson, R. Edwards, and D. Bathke (2001), Local to regional-scale variability of annual net accumulation on the Greenland ice sheet from PARCA cores, *J. Geophys. Res.*, *106*(D24), 33,839–33,851, doi:10.1029/2001JD900067.

Moy, C., G. Seltzer, D. Rodbell, and D. Anderson (2002), Variability of El Niño/Southern Oscillation activity at millennial timescales during the Holocene epoch, *Nature*, *420*(6912), 162–165, doi:10.1038/nature01194.

Mulvaney, R., N. Abram, R. Hindmarsh, C. Arrowsmith, L. Fleet, J. Triest, L. Sime, O. Alemany, and S. Foord (2012), Recent Antarctic Peninsula warming relative to Holocene climate and ice-shelf history, *Nature*, *489*(7414), 141–U204, doi:10.1038/nature11391.

Neale, R., J. Richter, S. Park, P. Lauritzen, S. Vavrus, P. Rasch, and M. Zhang (2013), The mean climate of the Community Atmosphere Model (CAM4) in forced SST and fully coupled experiments, *J. Clim.*, *26*(14), 5150–5168, doi:10.1175/JCLI-D-12-00236.1.

Novello, V. F., et al. (2012), Multidecadal climate variability in Brazil's Nordeste during the last 3000 years based on speleothem isotope records, *Geophys. Res. Lett.*, *39*, L23706, doi:10.1029/2012GL053936.

Oleson, K. W., et al. (2010), Technical description of version 4.0 of the Community Land Model (CLM), *NCAR Tech. Note NCAR/TN-478+STR*.

Olson, J., B. Baum, D. Cahoon, and J. Crawford (1999), Frequency and distribution of forest, savanna, and crop fires over tropical regions during PEM-Tropics A, *J. Geophys. Res.*, *104*(D5), 5865–5876, doi:10.1029/1998JD100066.

Painter, T., M. Flanner, G. Kaser, B. Marzeion, R. VanCuren, and W. Abdalati (2013), End of the Little Ice Age in the Alps forced by industrial black carbon, *Proc. Natl. Acad. Sci. U.S.A.*, *110*(38), 15,216–15,221, doi:10.1073/pnas.1302570110.

Pasteris, D., J. McConnell, R. Edwards, E. Isaksson, and M. Albert (2014a), Acidity decline in Antarctic ice cores during the Little Ice Age linked to changes in atmospheric nitrate and sea salt concentrations, *J. Geophys. Res. Atmos.*, *119*, 5640–5652, doi:10.1002/2013JD020377.

Pasteris, D., J. McConnell, S. Das, A. Criscitiello, M. Evans, O. Maselli, M. Sigl, and L. Layman (2014b), Seasonally resolved ice core records from West Antarctica indicate a sea ice source of sea-salt aerosol and a biomass burning source of ammonium, *J. Geophys. Res. Atmos.*, *119*, 9168–9182, doi:10.1002/2013JD020720.

Pereira, E., H. Evangelista, K. Pereira, I. Cavalcanti, and A. Setzer (2006), Apportionment of black carbon in the South Shetland Islands, Antarctic Peninsula, *J. Geophys. Res.*, *111*, D03303, doi:10.1029/2005JD006086.

Piovano, E. L., D. Ariztegui, F. Cordoba, M. Cioccale, and F. Sylvestre (2009), Hydrological variability in South America below the tropic of Capricorn (Pampas and Patagonia, Argentina) during the last 13.0 Ka, in *Past Climate Variability in South America and Surrounding Regions*, edited by F. Vimeux, F. Sylvestre, and M. Khodri, pp. 323–351, Springer, Netherlands.

Power, M. J., et al. (2008), Changes in fire regimes since the Last Glacial Maximum: An assessment based on a global synthesis and analysis of charcoal data, *Clim. Dyn.*, *30*(7–8), 887–907, doi:10.1007/s00382-007-0334-x.
Rhodes, R. H., X. Yang, E. W. Wolff, J. R. McConnell, and M. M. Frey (2017), Sea ice as a source of sea salt aerosol to Greenland ice cores: A model-based study, *Atmos. Chem. Phys. Discuss.*, doi:10.5194/acp-2017-100.
Sachs, J., D. Sachse, R. Smittenberg, Z. Zhang, D. Battisti, and S. Golubic (2009), Southward movement of the Pacific intertropical convergence zone AD 1400–1850, *Nat. Geosci.*, *2*(7), 519–525, doi:10.1038/ngeo554.
Shindell, D., and G. Faluvegi (2009), Climate response to regional radiative forcing during the twentieth century, *Nat. Geosci.*, *2*(4), 294–300, doi:10.1038/ngeo473.
Sigl, M., et al. (2014), Insights from Antarctica on volcanic forcing during the Common Era, *Nat. Clim. Change*, *4*(8), 693–697, doi:10.1038/nclimate2293.
Sigl, M., et al. (2015), Timing and climate forcing of volcanic eruptions for the past 2,500 years, *Nature*, *523*(7562), 543–549, doi:10.1038/nature14565.
Sigl, M., et al. (2016), The WAIS Divide deep ice core WD2014 chronology—Part 2: Annual-layer counting (0–31 ka BP), *Clim. Past*, *12*(3), 769–786, doi:10.5194/cp-12-769-2016.
Smith, R., et al. (2010), The Parallel Ocean Program (POP) reference manual: Ocean component of the Community Climate System Model (CCSM), *Tech. Rep., LAUR-10-01853*, Los Alamos Natl. Lab.
Thonicke, K., S. Venevsky, S. Sitch, and W. Cramer (2001), The role of fire disturbance for global vegetation dynamics: Coupling fire into a Dynamic Global Vegetation Model, *Global Ecol. Biogeogr.*, *10*(6), 661–677, doi:10.1046/j.1466-822x.2001.00175.x.
Thornton, P., J. Lamarque, N. Rosenbloom, and N. Mahowald (2007), Influence of carbon-nitrogen cycle coupling on land model response to CO_2 fertilization and climate variability, *Global Biogeochem. Cycles*, *21*, GB4018, doi:10.1029/2006GB002868.
van der Werf, G., J. Randerson, L. Giglio, N. Gobron, and A. Dolman (2008), Climate controls on the variability of fires in the tropics and subtropics, *Global Biogeochem. Cycles*, *22*, GB3028, doi:10.1029/2007GB003122.
Vuille, M., S. J. Burns, B. L. Taylor, F. W. Cruz, B. W. Bird, M. B. Abbott, L. C. Kanner, H. Cheng, and V. F. Novello (2012), A review of the South American monsoon history as recorded in stable isotopic proxies over the past two millennia, *Clim. Past*, *8*(4), 1309–1321, doi:10.5194/cp-8-1309-2012.
Wang, X., A. S. Auler, R. L. Edwards, H. Cheng, E. Ito, Y. Wang, X. Kong, and M. Solheid (2007), Millennial-scale precipitation changes in southern Brazil over the past 90,000 years, *Geophys. Res. Lett.*, *34*, L23701, doi:10.1029/2007GL031149.
Wang, Z., J. Chappellaz, K. Park, and J. Mak (2010), Large variations in Southern Hemisphere biomass burning during the last 650 years, *Science*, *330*(6011), 1663–1666, doi:10.1126/science.1197257.
Weller, R., A. Minikin, A. Petzold, D. Wagenbach, and G. König-Langlo (2013), Characterization of long-term and seasonal variations of black carbon (BC) concentrations at Neumayer, Antarctica, *Atmos. Chem. Phys.*, *13*, 1579–1590.
Wendl, I., J. Menking, R. Farber, M. Gysel, S. Kaspari, M. Laborde, and M. Schwikowski (2014), Optimized method for black carbon analysis in ice and snow using the Single Particle Soot Photometer, *Atmos. Meas. Tech.*, *7*(8), 2667–2681, doi:10.5194/amt-7-2667-2014.
Westerling, A., H. Hidalgo, D. Cayan, and T. Swetnam (2006), Warming and earlier spring increase western US forest wildfire activity, *Science*, *313*(5789), 940–943, doi:10.1126/science.1128834.
Wolff, E. W., and H. Cachier (1998), Concentrations and seasonal cycle of black carbon in aerosol at a coastal Antarctic station, *J. Geophys. Res.*, *103*(D9), 11,033–11,041, doi:10.1029/97JD01363.
Zennaro, P., et al. (2014), Fire in ice: Two millennia of boreal forest fire history from the Greenland NEEM ice core, *Clim. Past*, *10*(5), 1905–1924, doi:10.5194/cp-10-1905-2014.